

Bipartite and tripartite entanglement in the two-qubit quantum Rabi model

Lijun Mao(毛丽君), Hongmei Wang(王红梅), Yaoyao Zhou(周瑶瑶), and Hui Guo(郭慧)
Citation: Chin. Phys. B, 2026, 35 (**8**): 080303. DOI: 10.1088/1674-1056/ae85f7
http://cpb.iphy.ac.cn; http://iopscience.iop.org/cpb

What follows is a list of articles you may be interested in

Entanglement enhancement in a modulated optomechanical system via squeezed vacuum field

Huan-Huan Cheng(程欢欢), Chen-Rui Yang(杨晨锐), Gao-Feng Jiao(焦高锋), Cheng-Hua Bai(白成华), and Shao-Xiong Wu(武少雄)
Chin. Phys. B, 2026, 35 (**4**): 040311. DOI: 10.1088/1674-1056/ae2d37

Entanglement polygon inequalities for a class of mixed states

Xian Shi(石现)
Chin. Phys. B, 2024, 33 (**11**): 110308. DOI: 10.1088/1674-1056/ad8eb0

Commensurate and incommensurate Haldane phases for a spin-1 bilinear-biquadratic model

Yan-Wei Dai(代艳伟), Ai-Min Chen(陈爱民), Xi-Jing Liu(刘希婧), and Yao-Heng Su(苏耀恒)
Chin. Phys. B, 2023, 32 (**9**): 090304. DOI: 10.1088/1674-1056/acac0c

Unified entropy entanglement with tighter constraints on multipartite systems

Qi Sun(孙琪), Tao Li(李陶), Zhi-Xiang Jin(靳志祥), and Deng-Feng Liang(梁登峰)
Chin. Phys. B, 2023, 32 (**3**): 030304. DOI: 10.1088/1674-1056/aca399

Quantum entanglement dynamics based oncomposite quantum collision model

Xiao-Ming Li(李晓明), Yong-Xu Chen(陈勇旭), Yun-Jie Xia(夏云杰), Qi Zhang(张琦), Zhong-Xiao Man(满忠晓)
Chin. Phys. B, 2020, 29 (**6**): 060302. DOI: 10.1088/1674-1056/ab84d0

Bipartite and tripartite entanglement in the two-qubit quantum Rabi model

Lijun Mao(毛丽君)†, Hongmei Wang(王红梅), Yaoyao Zhou(周瑶瑶), and Hui Guo(郭慧)

Department of Physics, Taiyuan Normal University, Jinzhong 030619, *China*

(Received 24 February 2026; revised manuscript received 16 May 2026; accepted manuscript online 3 July 2026)

This study investigates the entanglement dynamics of the two-qubit quantum Rabi model (QRM) with both homogeneous and inhomogeneous couplings using the adiabatic approximation. The quantized field is initially prepared in a coherent state, while a separable state and a maximally entangled Bell state are selected as the initial two-qubit states. We characterize distinct types of entanglement generated among the subsystems through qubit–field interactions, with a focus on the bipartite entanglement between a single qubit and the field. Building on this, we examine tripartite correlations through the I-residual tangle, a measure that conclusively verifies the presence of genuine tripartite entanglement among the two qubits and the field. This work provides insights into the generation of tunable multipartite entanglement and the detection of quantum phase transitions in light–matter systems, such as circuit quantum electrodynamics (QED).

Keywords: I-residual tangle, tripartite entanglement, bipartite entanglement, two-qubit QRM

PACS: 03.65.Ud, 42.50.Pq, 42.50.Md

DOI: 10.1088/1674-1056/ae85f7 **CSTR:** 32038.14.CPB.ae85f7

1. Introduction

The coupling of a single qubit to a quantized single-mode field is described by the quantum Rabi model (QRM),[1,2] which is of fundamental importance in both theoretical and experimental studies across various areas of physics, such as atomic physics, quantum optics, and mesoscopic physics.[3–5] The Jaynes–Cummings (JC) model[6] can be derived directly by applying the rotating-wave approximation to the QRM. Of particular interest is the ultrastrong coupling regime, which has been experimentally realized in modern quantum technologies such as superconducting circuits and semiconductor nanostructures.[7–9] In this regime, the rotating-wave approximation fails to capture essential quantum effects, and the counter-rotating terms become crucial, giving rise to rich quantum phenomena that are absent in the JC model.[10–12] Moreover, extended versions of the QRM have found broad applications in cavity and circuit quantum electrodynamics (QED), as well as semiconductor systems. These include the Dicke model,[13,14] the two-photon interaction system,[15,16] the anisotropic QRM,[17,18] the multi-qubit QRM,[19–25] the multilevel QRM,[26–28] and the asymmetric QRM.[29–32]

Quantum entanglement and coherence are fundamental concepts in quantum mechanics and serve as essential resources for quantum technologies.[33] Notable advancements have been achieved in high-fidelity two-qubit gate operations,[34–37] where the key requirement is the generation of entanglement between two spatially separated qubits. Cavity-mediated qubit interactions provide a powerful platform for engineering such entanglement between qubit pairs.[38,39] Moreover, other types of entanglement, including multipartite entanglement, can exist in such interacting systems.[40] However, most existing studies concentrate on bipartite entanglement between subsystems of multipartite systems. Genuine multipartite entanglement, which cannot be decomposed into entanglement across any bipartition, remains less explored. This motivates a comprehensive investigation of both bipartite and genuine multipartite entanglement in cavity-mediated qubit systems. The two-qubit QRM, where two qubits are coupled to a common cavity mode, serves as the simplest yet nontrivial platform for such studies.

In this paper, we focus on the entanglement dynamics of the two-qubit QRM, including entanglement across different bipartite partitions and genuine tripartite entanglement. The total Hilbert space has a tensor product structure $\mathbb{C}^2\otimes\mathbb{C}^2\otimes\mathcal{H}_\infty$ (with $\dim(\mathcal{H}_\infty)=\infty$), corresponding to two qubits and a quantized field, respectively. We consider initial states of the form $|\psi(0)\rangle = |\phi_{\rm q}\rangle\otimes|z\rangle$, where the field is prepared in a coherent state and the qubits are initialized in either a separable state or a maximally entangled Bell state. Using the adiabatic approximation, we derive explicit analytical expressions for the dynamical evolution of the system, enabling a detailed characterization of its entanglement distribution.

In our quantum dynamical analysis, we neglect measurement backaction and environmental decoherence, thereby assuming that the tripartite quantum system remains in a pure state throughout its evolution. However, the reduced state of the bipartite subsystem consisting of a single qubit and the field generally evolves into a mixed state in the Hilbert space

†Corresponding author. E-mail: maolijun516@163.com

© 2026 Chinese Physical Society and IOP Publishing Ltd. All rights, including for text and data mining, AI training, and similar technologies, are reserved.

$\mathbb{C}^2 \otimes \mathcal{H}_\infty$. For such a partition, the tangle proposed by Wootters *et al.*[41,42] for two qubits is inapplicable. Fortunately, Osborne's work[43] provides an analytic formulation of the *I*-tangle applicable to this case. Thus, we quantify pairwise entanglement for several possible subsystem partitions of the tripartite system. Notably, genuine tripartite entanglement can be characterized by a generalized residual tangle, revealing the constraints imposed by entanglement sharing on the values of various bipartite tangles. By shifting the focus from cavity-mediated entanglement between two qubits to field-involving bipartitions and tripartite entanglement, we systematically characterize entanglement evolution in the two-qubit QRM. This analysis has significant implications for entanglement generation and quantum control in light–matter systems, with potential applications in quantum information processing.

2. Eigenstates and eigenenergies

The Hamiltonian of the two-qubit QRM is given by (we set $\hbar = 1$)[1]

$$H = \omega_c a^\dagger a + \sum_{j=1,2}\left[-\frac{\omega_j}{2}\sigma_j^x + g_j\left(a^\dagger + a\right)\sigma_j^z\right], \tag{1}$$

where $a^\dagger$ and a denote the creation and annihilation operators, respectively, of a single bosonic mode with frequency ω_c, σ_j^k ($k = x, y, z$) are the Pauli matrices for the j-th qubit, and g_j characterizes the dipole-field coupling strength between qubit j and the field. Let $|1\rangle_j$ and $|0\rangle_j$ denote the eigenstates of σ_j^z corresponding to the eigenvalues $+1$ (upper) and -1 (lower), respectively. The basis states of a two-qubit system can be expressed as $|11\rangle = |1\rangle_1 \otimes |1\rangle_2$, $|10\rangle = |1\rangle_1 \otimes |0\rangle_2$,, $|01\rangle = |0\rangle_1 \otimes |1\rangle_2$, and $|00\rangle = |0\rangle_1 \otimes |0\rangle_2$. Accordingly, we define four displaced bosonic operators $A_i^\dagger = a^\dagger + \beta_i$ and $A_i = a + \beta_i$ ($i = 1, 2, 3, 4$), such that the corresponding displaced number states satisfy $A_i^\dagger A_i |n\rangle_{A_i} = n|n\rangle_{A_i}$. The displacement parameters are determined by the qubit–field interaction and are given by $\beta_1 = -\beta_4 = (g_2 + g_1)/\omega_c$ and $\beta_2 = -\beta_3 = (g_1 - g_2)/\omega_c$.

In the displaced Fock basis, as shown in our previous work, the adiabatic approximation provides a powerful framework for deriving analytical solutions when the qubit frequencies are much smaller than the field frequency. The Hamiltonian becomes approximately block diagonal, with each photon number corresponding to a 4×4 block that further decomposes into two 2×2 submatrices associated with the even-parity ($\kappa = +$) and odd-parity ($\kappa = -$) subspaces.[44] The resulting block Hamiltonian reads

$$H_m^\kappa = \begin{pmatrix} \varepsilon_{1m} & \Omega_m^\kappa \\ \Omega_m^\kappa & \varepsilon_{2m} \end{pmatrix}, \tag{2}$$

where $\varepsilon_{im} = \left(m - \beta_i^2\right)\omega_c$. The off-diagonal terms, which describe transitions between states within the same block, are given by

$$\Omega_m^\kappa = -\frac{\omega_2}{2} A_1\langle m|m\rangle_{A_2} - \frac{\omega_1}{2}\chi_{A_1}\langle m|m\rangle_{A_3},$$

where $\chi = \kappa(-1)^m$. The overlap integral is expressed as

$${}_{A_i}\langle m|m\rangle_{A_j} = \mathrm{e}^{-\beta_{ij}^2/2}\sum_{l=0}^{m}\frac{(-1)^{m-l}m!}{l![(m-l)!]^2}\beta_{ij}^{2(m-l)}.$$

Diagonalizing Eq. (2) yields the eigenvalues

$$E_m^{\kappa\pm} = m\omega_c - \left(\beta_1^2 + \beta_2^2\right)\omega_c/2 \pm \theta_m^\kappa, \tag{3}$$

with $\theta_m^\kappa = \sqrt{(\Omega_m^\kappa)^2 + \omega_c^2\left(\beta_1^2 - \beta_2^2\right)^2/4}$. The corresponding eigenstates, exploiting the symmetry relations among the expansion coefficients, can be written as

$$\left|\psi_m^{\kappa\pm}\right\rangle = \frac{1}{\sqrt{2}}\begin{pmatrix} d_{1m}^{\kappa\pm} \\ d_{2m}^{\kappa\pm} \\ \chi d_{2m}^{\kappa\pm} \\ \chi d_{1m}^{\kappa\pm} \end{pmatrix}, \tag{4}$$

where

$$d_{1m}^{\kappa\pm} = \xi_m^{\kappa\pm}\sqrt{\frac{1}{1+\left(\xi_m^{\kappa\pm}\right)^2}}, \quad d_{2m}^{\kappa\pm} = -\sqrt{\frac{1}{1+\left(\xi_m^{\kappa\pm}\right)^2}},$$

with $\xi_m^{\kappa\pm} = \Omega_m^\kappa / \left[\left(\beta_2^2 - \beta_1^2\right)\omega_c/2 \mp \theta_m^\kappa\right]$.

In the case of identical qubits ($\omega_1 = \omega_2 = \omega$, $g_1 = g_2 = g$), the off-diagonal term reduces to the form $\Omega_m^\kappa = -\frac{\omega}{2} A_1\langle m|m\rangle_{A_2}\left(1+\chi\right)$. It vanishes for odd m in the even-parity subspace and for even m in the odd-parity subspace, yielding the eigenvalues

$$E_m^{\kappa+} = m\omega_c, \quad E_m^{\kappa-} = \left(m - \beta_1^2\right)\omega_c,$$

whose eigenstates take the form $|\psi_m^{\kappa+}\rangle = |\psi_1\rangle$ and $|\psi_m^{\kappa-}\rangle = |\psi_2\rangle$, where

$$|\psi_1\rangle = \frac{1}{\sqrt{2}}\begin{pmatrix} 0 \\ 1 \\ -1 \\ 0 \end{pmatrix}, \quad |\psi_2\rangle = \frac{1}{\sqrt{2}}\begin{pmatrix} 1 \\ 0 \\ 0 \\ -1 \end{pmatrix}. \tag{5}$$

For the case of a nonzero off-diagonal term Ω_m^κ, assuming the condition $|\Omega_m^\kappa|/\omega_c \gg \beta_1^2$ as reported in Ref. [45], the eigenvalues simplify to $E_m^{\kappa+} = m\omega_c + \Omega_m^\kappa$ and $E_m^{\kappa-} = m\omega_c - \Omega_m^\kappa$, with the corresponding eigenstates $|\psi_m^{\kappa+}\rangle = |\psi_3\rangle$ and $|\psi_m^{\kappa-}\rangle = |\psi_4\rangle$, where

$$|\psi_3\rangle = \frac{1}{2}\begin{pmatrix} 1 \\ 1 \\ 1 \\ 1 \end{pmatrix}, \quad |\psi_4\rangle = \frac{1}{2}\begin{pmatrix} 1 \\ -1 \\ -1 \\ 1 \end{pmatrix}. \tag{6}$$

3. Entanglement dynamics

The interaction between the field and the ensemble of qubits induces entanglement among the subsystems in the two-qubit QRM. Based on the analytical results derived above, we investigate the entanglement dynamics within the ultrastrong coupling regime. The initial states are assumed to be pure product states of the field and the two-qubit subsystem. To capture the essential features of bipartite and tripartite entanglement evolution, we consider two types of initial states

$$|\Psi^{\mathrm{s}}(0)\rangle = |10\rangle|z\rangle, \quad |\Psi^{\mathrm{e}}(0)\rangle = (|10\rangle + |01\rangle)|z\rangle/\sqrt{2},$$

where the field is in a coherent state characterized by an average photon number $|z|^2$, and the two qubits are in a separable state or a Bell state, respectively.

Within the adiabatic approximation, the time-evolved state can be expanded in the eigenbasis $\{|\psi_m^{\kappa\gamma}\rangle\}$. For small β_1, the Fock state $|m\rangle$ can be expanded in the displaced Fock space. The dominant contribution comes from the terms with the same m, corresponding to the state approximation $|m\rangle \approx |m\rangle_{A_i}$. Thus, for the initial separable state, we obtain the time-evolved state

$$|\Psi^{\mathrm{s}}(t)\rangle = \frac{1}{\sqrt{2}}\sum_{m=0}^{\infty}\sum_{\kappa,\gamma=\pm} \mathrm{e}^{\frac{-|z|^2}{2}}\frac{z^m}{\sqrt{m!}}d_{2m}^{\kappa\gamma}|\psi_m^{\kappa\gamma}\rangle\,\mathrm{e}^{-\mathrm{i}E_m^{\kappa\gamma}t}.$$

The reduced density matrix of the two-qubit subsystem is obtained by tracing out the cavity field, $\rho_{12}^{\mathrm{s}}(t) = \mathrm{Tr}_F\left[|\Psi^{\mathrm{s}}(t)\rangle\langle\Psi^{\mathrm{s}}(t)|\right]$. For a system of two identical qubits, substituting the simplified eigen-solutions (5) and (6) into $|\Psi^{\mathrm{s}}(t)\rangle$ allows us to derive the reduced density matrix of the qubits

$$\rho_{12}^{\mathrm{s}}(t) = \sum_{m,\kappa}\frac{p(m)(1+\chi)}{16}\begin{pmatrix} c_{1m}^{\kappa} & -c_{2m}^{\kappa+} & -c_{2m}^{\kappa-} & c_{1m}^{\kappa} \\ c_{2m}^{\kappa+} & c_{3m}^{\kappa+} & -c_{1m}^{\kappa} & c_{2m}^{\kappa+} \\ c_{2m}^{\kappa-} & -c_{1m}^{\kappa} & c_{3m}^{\kappa-} & c_{2m}^{\kappa-} \\ c_{1m}^{\kappa} & -c_{2m}^{\kappa+} & -c_{2m}^{\kappa-} & c_{1m}^{\kappa} \end{pmatrix}, \quad (7)$$

where the normalized Poisson distribution is defined as $p(m) = \mathrm{e}^{-|z|^2}|z|^{2m}/m!$. The explicit forms of the matrix elements are given as follows:

$$\begin{aligned} c_{1m}^{\kappa} &= 1-\cos(2\Omega_m^{\kappa}t), \\ c_{2m}^{\kappa\pm} &= \mathrm{i}\sin(2\Omega_m^{\kappa}t) \pm 2\mathrm{i}\sin(\Omega_m^{\kappa}t), \\ c_{3m}^{\kappa\pm} &= 3+\cos(2\Omega_m^{\kappa}t) \pm 4\cos(\Omega_m^{\kappa}t). \end{aligned}$$

Rungta *et al.*[46] proposed the I-concurrence, a good bipartite entanglement measure for a joint pure state $|\psi\rangle_{AB}$. It generalizes the concept of concurrence from two-qubit systems to systems with arbitrary dimensions. The I-tangle, defined as the square of the I-concurrence, is given by

$$\tau_{A,B} = 2\left[1-\mathrm{tr}\left(\rho_A^2\right)\right]. \quad (8)$$

The pure-state I-tangle ranges from zero for product states to $2(n-1)/n$ for maximally entangled states, where n is the smaller dimension of the two subsystems. Substituting the time-evolved density matrix $\rho_{12}^{\mathrm{s}}(t)$ into Eq. (8) yields the bipartite I-tangle $\tau_{F,12}^{\mathrm{s}}(t)$. This quantity quantifies the entanglement between the field (F) and the joint qubit pair (12), referred to as type-(i) entanglement. In the limit $|\beta_1 z| \ll 1$, only the first three terms (corresponding to $l = m$, $m-1$, and $m-2$) in the summation appearing in the expression for Ω_m^{κ} need to be retained.[45] We derive an analytical expression for $\tau_{F,12}^{\mathrm{s}}(t)$, i.e.,

$$\tau_{F,12}^{\mathrm{s}}(t) = \frac{5-|S(t,2\omega)|^2-4|S(t,\omega)|^2}{4}. \quad (9)$$

Furthermore, the reduced density matrix of qubit 2, $\rho_2^{\mathrm{s}}(t)$, is obtained by tracing out qubit 1 from $\rho_{12}^{\mathrm{s}}(t)$. This allows us to calculate the I-tangle $\tau_{F1,2}^{\mathrm{s}}(t)$, which measures the bipartite entanglement between the composite subsystem (field + qubit 1) and qubit 2. We label this as type-(ii) entanglement, which for an identical qubit system is given by

$$\tau_{F1,2}^{\mathrm{s}}(t) = 1-|S(t,\omega)|^2. \quad (10)$$

Equations (9) and (10) reveal the explicit oscillatory behavior of both entanglement measures. The oscillatory function $S(t,\omega)$ is defined as $S(t,\omega) = \sum_{k=0}^{\infty}S_k(t,\omega)$, where each component takes the form $S_k(t,\omega) = h_k\exp(\Phi_{\mathrm{Re}}+\mathrm{i}\Phi_{\mathrm{Im}})$. The terms are defined as follows: the amplitude $h_k = \left(1+\pi^2k^2f^2\right)^{-1/4}$, the envelope factor $\Phi_{\mathrm{Re}} = -\frac{1}{2}h_k^4(\mu-\mu_k)^2 f\beta_1^2$, and the oscillatory phase $\Phi_{\mathrm{Im}} = \frac{1}{2}\tan^{-1}(\pi kf)+\mu(1-f)+2\pi k|z|^2$. The auxiliary parameters are $f = |z|^2\beta_1^2$, $\mu = \omega t\,\mathrm{e}^{-\beta_1^2/2}$, and $\mu_k = 2\pi k(1+f/2)/\beta_1^2$.

In addition, the initially non-entangled qubit pair may evolve into an entangled mixed state. The bipartite entanglement between the two qubits is named type-(iii) entanglement and can be quantified by the tangle, defined as the square of the concurrence,[41,42] i.e.,

$$\tau_{1,2}^{\mathrm{s}} = \left(\max\{0,\lambda_1-\lambda_2-\lambda_3-\lambda_4\}\right)^2, \quad (11)$$

where λ_i are the square roots of the eigenvalues (in decreasing order) of the matrix $\rho_{12}\tilde{\rho}_{12}$. Here, $\tilde{\rho}_{12} = (\sigma_y\otimes\sigma_y)\rho_{12}^*(\sigma_y\otimes\sigma_y)$, and all λ_i are real and non-negative.

The last type of bipartite tangle corresponds to the entanglement between a single qubit (e.g., qubit 1) and the field, referred to as type-(iv) entanglement. Tracing the pure-state density operator over qubit 2 and qubit 1 yields the reduced density matrices $\rho_{F1}^{\mathrm{s}}(t)$ and $\rho_{F2}^{\mathrm{s}}(t)$, respectively:

$$\begin{aligned} \rho_{F1}^{\mathrm{s}}(t) &= \mathrm{Tr}_2\left(|\Psi^{\mathrm{s}}(t)\rangle\langle\Psi^{\mathrm{s}}(t)|\right), \\ \rho_{F2}^{\mathrm{s}}(t) &= \mathrm{Tr}_1\left(|\Psi^{\mathrm{s}}(t)\rangle\langle\Psi^{\mathrm{s}}(t)|\right). \end{aligned}$$

This bipartite subsystem is described by a Hilbert space $\mathbb{C}^2\otimes\mathcal{H}_\infty$ and generally evolves into a mixed state. The previously mentioned I-tangles are not directly applicable to arbitrary

mixed states. However, since the tripartite system remains pure at all times, the Schmidt decomposition theorem[47] indicates that the reduced density operator $\rho^{\rm s}_{F1}(t)$ has a maximum rank of 2. This bound is determined by the minimum subsystem dimension, which in this partition corresponds to the two-level system (qubit 2). Osborne's formula provides a method to quantify the entanglement of mixed states for a bipartite system AB via the I-tangle.[43] This formula, which generalizes the entanglement measure to rank-2 mixed states, is given by

$$\tau_{A,B} = \mathrm{tr}\left(\rho_{AB}\tilde{\rho}_{AB}\right) + 2\lambda_{\min}^{(AB)}\left(1 - \mathrm{tr}\left(\rho_{AB}^2\right)\right). \tag{12}$$

The spin-flip operation for ρ_{AB} is defined as $\tilde{\rho}_{AB} \equiv I_A \otimes I_B - \rho_A \otimes I_B - I_A \otimes \rho_B + \rho_{AB}$, where $\rho_A = \mathrm{tr}_B(\rho_{AB})$ and $\rho_B = \mathrm{tr}_A(\rho_{AB})$ are the reduced density matrices. $\lambda_{\min}^{(AB)}$ is the smallest eigenvalue of the real symmetric 3×3 matrix M introduced by Osborne.[43] The explicit form of the matrix M is constructed from the eigensystem of ρ_{AB}. By substituting the reduced density matrices $\rho^{\rm s}_{F1}(t)$ and $\rho^{\rm s}_{F2}(t)$ into Eq. (12), we obtain the I-tangles $\tau^{\rm s}_{F,1}(t)$ and $\tau^{\rm s}_{F,2}(t)$, respectively. Thus, we have studied the I-tangles for various distinct bipartite partitions in the two-qubit QRM.

Crucially, the tangles associated with distinct bipartite partitions in the two-qubit QRM are not independent but are subject to specific constraints quantified by the I-residual tangle,[47] which is defined as

$$\begin{aligned}\tau_{ABC} &= \frac{1}{3}\left(\tau_{A,BC} + \tau_{AB,C} + \tau_{AC,B}\right)\\ &\quad -\frac{2}{3}\left(\tau_{A,B} + \tau_{A,C} + \tau_{B,C}\right).\end{aligned} \tag{13}$$

The I-residual tangle represents the average loss of bipartite entanglement in a tripartite system when any one of the subsystems is traced out. It can be regarded as irreducible tripartite entanglement, since it cannot be quantified by any combination of bipartite entanglement measures. Note that the expression (13) has been verified for a tripartite system with the structure $\mathbb{C}^2\otimes\mathbb{C}^2\otimes\mathcal{H}_\infty$ in an overall pure state. Consequently, this formula is well suited for quantifying the tripartite entanglement $\tau^{\rm s}_{F12}(t)$ in the two-qubit QRM when the system starts from a separable state.

When the qubits are initially prepared in a Bell state, we follow the same procedure. Through a unitary transformation, the reduced density operator of the two-qubit subsystem takes a simplified form in the eigenbasis of the spin product operator $\sigma_1^x \otimes \sigma_2^x$

$$\rho^{\rm e}_{12}(t) = \sum_{m,\kappa}\frac{p(m)(1+\chi)}{4}\begin{pmatrix} q_{1m}^{\kappa+} & 0 & 0 & q_{2m}^{\kappa+}\\ 0 & 0 & 0 & 0\\ 0 & 0 & 0 & 0\\ q_{2m}^{\kappa-} & 0 & 0 & q_{1m}^{\kappa-}\end{pmatrix}, \tag{14}$$

where the coefficients $q_{1m}^{\kappa\pm}$ and $q_{2m}^{\kappa\pm}$ are defined as

$$\begin{aligned} q_{1m}^{\kappa\pm} &= 1 \pm \frac{4\xi_m^{\kappa+}\left(\left(\xi_m^{\kappa+}\right)^2 - 1\right)\sin^2\left(\theta_m^{\kappa}t\right)}{\left(\left(\xi_m^{\kappa+}\right)^2 + 1\right)^2},\\ q_{2m}^{\kappa\pm} &= -1 + \frac{8\left(\xi_m^{\kappa+}\right)^2\sin^2\left(\theta_m^{\kappa}t\right)}{\left(\left(\xi_m^{\kappa+}\right)^2 + 1\right)^2} \mp i\frac{2\xi_m^{\kappa+}\sin\left(2\theta_m^{\kappa}t\right)}{\left(\xi_m^{\kappa+}\right)^2 + 1}.\end{aligned}$$

For this initial state, the reduced density matrix $\rho^{\rm e}_{12}(t)$ belongs to a special class of density matrices (X-matrices), for which only the diagonal and anti-diagonal elements are nonzero. This structure yields analytical expressions for entanglement measures even for inhomogeneous coupling. Two of the corresponding pure-state I-tangles can be written as

$$\tau^{\rm e}_{F,12}(t) = 2 - \sum_{m,m',\kappa,\kappa'}\frac{p(m)p(m')(1+\chi)(1+\chi')}{8}\left(q_{1m}^{\kappa+}q_{1m'}^{\kappa'+} + q_{2m}^{\kappa+}q_{2m'}^{\kappa'-} + q_{2m}^{\kappa-}q_{2m'}^{\kappa'+} + q_{1m}^{\kappa-}q_{1m'}^{\kappa'-}\right), \tag{15}$$

$$\tau^{\rm e}_{F1,2}(t) = 2 - \sum_{m,m',\kappa,\kappa'}\frac{p(m)p(m')(1+\chi)(1+\chi')}{8}\left(q_{1m}^{\kappa+}q_{1m'}^{\kappa'+} + q_{1m}^{\kappa-}q_{1m'}^{\kappa'-}\right). \tag{16}$$

When the two qubits are identical in the model, the two expressions can be simplified as

$$\tau^{\rm e}_{F,12}(t) = 1 - |S(t,2\omega)|^2, \tag{17}$$

$$\tau^{\rm e}_{F1,2}(t) = 1. \tag{18}$$

Similarly, the two-qubit tangle can be expressed as

$$\tau^{\rm e}_{1,2}(t) = \left|\sum_{m=0}^{\infty}\sum_{\kappa=\pm}\frac{p(m)(1+\chi)}{2}q_{2m}^{\kappa+}\right|^2, \tag{19}$$

which, for identical qubits, reduces to

$$\tau^{\rm e}_{1,2}(t) \approx |S(t,2\omega)|^2. \tag{20}$$

By tracing out the respective qubits from the total pure state, we obtain the reduced density matrices $\rho^{\rm e}_{F1}(t)$ and $\rho^{\rm e}_{F2}(t)$. Substituting these matrices into Eq. (12) allows us to derive the entanglement between a single qubit and the field ($\tau^{\rm e}_{F,1}(t)$ and $\tau^{\rm e}_{F,2}(t)$) for the initial Bell state. With various types of bipartite entanglement established, we employ the I-residual tangle $\tau^{\rm e}_{F12}(t)$ (defined by Eq. (13)) to quantify the genuine tripartite entanglement.

Figures 1–3 present distinct types of bipartite entanglement for two different initial states, including the inhomogeneous coupling case in Fig. 1 and the homogeneous coupling case in Figs. 2 and 3. The type-(i) entanglement $\tau^{\rm s}_{F,12}(t)$

is initially zero for the initial separable state, as shown in Figs. 1(a1), 2(a1), and 3(a1). Due to the interaction, it rapidly reaches its maximum value, which is close to the theoretical limit of 1.5. Only irregular small-amplitude fluctuations occur during the subsequent evolution for inhomogeneous coupling. Notably, it maintains sustained high-level entanglement between the field and the two qubits. In contrast, under perfectly homogeneous coupling, it has the explicit form given in Eq. (9), where the fundamental term $S(t,\omega)$ exhibits periodic revivals. Each constituent $S_k(t,\omega)$ in the summation is centered at the k-th revival time, $t_k = \frac{\mu_k}{\omega}\mathrm{e}^{\beta_1^2/2}$. When these revivals are well resolved and non-overlapping, interference between the various k terms in the sum becomes negligible, allowing us to focus solely on the revival envelope. Consequently, the revival envelope and height are determined by the factors $\exp(\Phi_{\mathrm{Re}})$ and h_k, respectively.

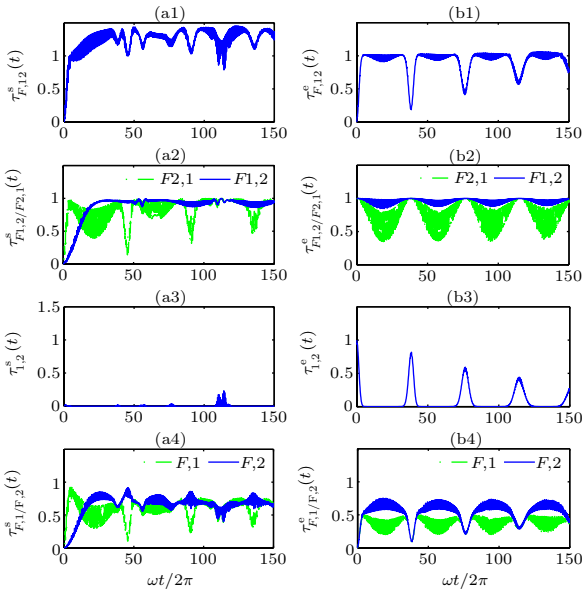


Fig. 1. Time evolution of bipartite I-tangles for the initial separable (left column) and Bell (right column) states. Parameters: $\omega_1 = \omega_2 = \omega = 0.15\omega_c$, $z = 3$, and inhomogeneous coupling with $g_1 = 0.08\omega_c$ and $g_2 = 0.03\omega_c$. All results are obtained within the adiabatic approximation.

The entanglement measure $\tau^{\mathrm{s}}_{F,12}(t)$ in Eq. (9) decreases linearly with the squared magnitudes of the fundamental and second-harmonic components, $|S(t,\omega)|^2$ and $|S(t,2\omega)|^2$. In Fig. 2(a1), the revival period of $S(t,\omega)$ is relatively long, and only a single shallow dip is observed at time $t_1/2$. Conversely, the shortened period of $S(t,\omega)$ with increasing coupling strength leads to deep dips in $\tau^{\mathrm{s}}_{F,12}(t)$ at discrete times t_k, with shallower dips occurring midway between consecutive t_k, as shown in Fig. 3(a1). The modulation is primarily determined by the prefactors in Eq. (9), with the fundamental term contributing four times as much as the second-harmonic counterpart. The decreasing amplitude of the dips is attributed to the reduction of h_k with increasing index k and coupling strength.

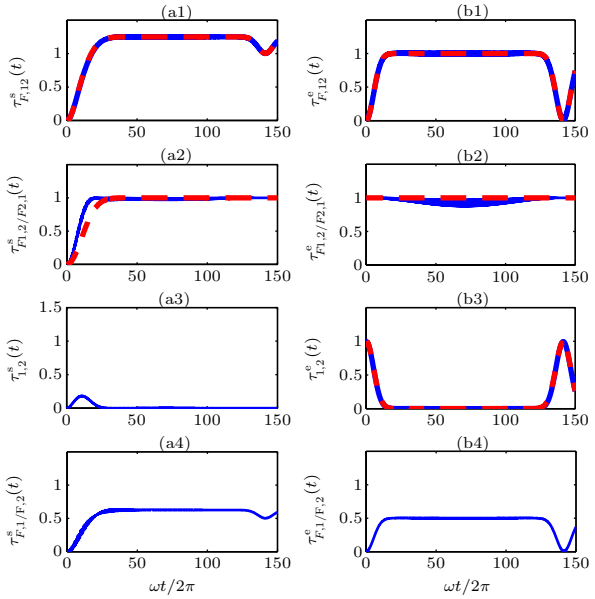


Fig. 2. Time evolution of bipartite I-tangles for the initial separable (left column) and Bell (right column) states. Parameters: $\omega_1 = \omega_2 = \omega = 0.15\omega_c$, $z = 3$, and homogeneous coupling with $g_1 = g_2 = 0.03\omega_c$. Results obtained from the adiabatic approximation (blue solid curves) and the analytical solution (red dashed curves) are shown.

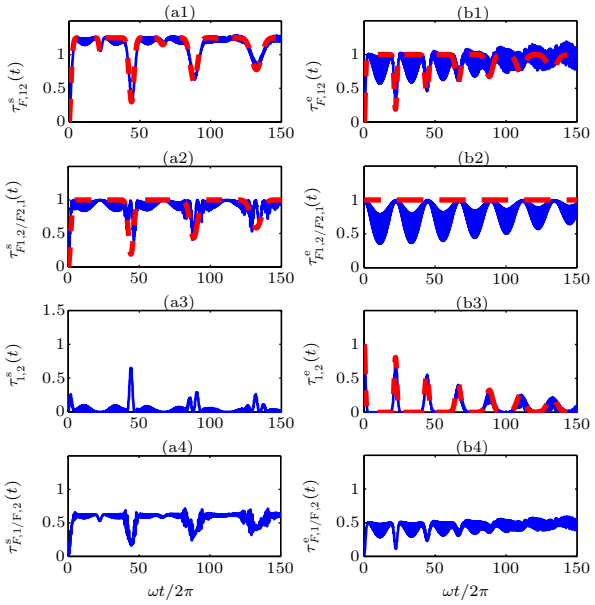


Fig. 3. Time evolution of bipartite I-tangles for the initial separable (left column) and Bell (right column) states under homogeneous coupling with enhanced strength $g_1 = g_2 = 0.08\omega_c$. Other parameters are identical to those in Fig. 2. Results obtained from the adiabatic approximation (blue solid curves) and the analytical solution (red dashed curves) are shown.

The intrinsic entanglement of Bell states suppresses the maximum value of the I-tangle $\tau^{\mathrm{e}}_{F,12}(t)$ relative to $\tau^{\mathrm{s}}_{F,12}(t)$, as evidenced in Figs. 1(b1), 2(b1), and 3(b1). Specifically, due to the symmetry of the Bell state, $\tau^{\mathrm{e}}_{F,12}(t)$ described by Eq. (17) exhibits second-harmonic oscillations for homogeneous coupling. The dips occur at times $t_k/2$. Furthermore, the system governed by Eq. (15) also exhibits periodic oscillations for inhomogeneous coupling. The period lies between those of the homogeneous cases with coupling strengths g_1 and g_2. Overall, the analytical predictions (red dashed curves) for the type-

(i) entanglement show good agreement with the envelopes obtained from the adiabatic approximation (blue solid curves) for both initial states.

For the initial separable state in Figs. 1(a2), 2(a2), and 3(a2), the type-(ii) entanglement rises from zero to its theoretical maximum of 1. Subsequently, for inhomogeneous coupling, $\tau^{\rm s}_{F2,1}(t)$ (green dash-dotted curve) exhibits deep dips interspersed with rapid small-amplitude oscillations, while $\tau^{\rm s}_{F1,2}(t)$ (blue solid curve) remains stable despite minor fluctuations. As the coupling strengths increase, the I-tangle $\tau^{\rm s}_{F1,2}(t)$ described by Eq. (10) changes from being saturated at its maximum value to developing pronounced oscillations with minima at discrete times t_k, as shown in Figs. 2(a2) and 3(a2). For the initial Bell state in Fig. 1(b2), $\tau^{\rm e}_{F1,2}(t)$ (blue solid curve) maintains excellent stability, while $\tau^{\rm e}_{F2,1}(t)$ (green dash-dotted curve) displays only rapid oscillations without deep dips. The I-tangle $\tau^{\rm e}_{F1,2}(t)$ described by Eq. (18) remains nearly unity for homogeneous coupling, as shown in Fig. 2(b2). However, the emergence of rapid oscillations in Fig. 3(b2) signifies a breakdown of this description, rendering the analytical solution invalid in the ultrastrong coupling regime. Specifically, the stable behavior under strong coupling contrasts with the pronounced fluctuations induced by ultrastrong coupling.

Panels (a3) and (b3) of Figs. 1–3 show the type-(iii) entanglement. The I-tangle $\tau^{\rm s}_{1,2}(t)$ for the initial separable state exhibits pronounced peaks only at sparse discrete times under ultrastrong coupling of both qubits. This demonstrates that the generation of two-qubit entanglement from such an initial state relies on sufficiently strong coupling. However, the I-tangle $\tau^{\rm e}_{1,2}(t)$ corresponding to the initial Bell state exhibits periodic collapse and revival dynamics in Figs. 1(b3), 2(b3), and 3(b3). As derived from Eq. (20), these revivals occur at times $t_k/2$ in the homogeneous coupling case. The initial entanglement of the Bell state is not irreversibly lost and undergoes partial recovery during the evolution. Furthermore, the entanglement between the field and the two qubits never attains its theoretical maximum. Thus, the initial Bell state exhibits strong robustness against the qubit-field interaction.

We now examine the dynamics of type-(iv) entanglement. Notably, our numerical analysis reveals the equality

$$\tau_{F,1}(t)+\tau_{F,2}(t)=\tau_{F,12}(t), \tag{21}$$

which holds for both initial states. The entanglement between the field and two qubits is fully described by the sum of the individual qubit-field entanglement components. In Fig. 1(a4), $\tau^{\rm s}_{F,1}(t)$ for the initial separable state exhibits obvious deep dips under inhomogeneous coupling, which are synchronized with the minor peaks of $\tau^{\rm s}_{F,2}(t)$. Their collective behavior generates a high-level small-amplitude oscillatory mode in $\tau^{\rm s}_{F,12}(t)$. However, for the initial Bell state in Fig. 1(b4), $\tau^{\rm e}_{F,1}(t)$ and $\tau^{\rm e}_{F,2}(t)$ exhibit deep dips synchronously. At other times, they display complementary behavior: one exceeds 0.5 at the expense of the other, ensuring that their sum never exceeds the maximum value of $\tau^{\rm e}_{F,12}(t)$. For the homogeneous coupling cases shown in Figs. 2(a4), 2(b4), 3(a4), and 3(b4), the I-tangle for single qubit-field entanglement is consistently half that of the field and two qubits, with both following the same evolutionary pattern. Throughout the evolution, two-qubit entanglement revives at the expense of qubit-field entanglement for the initial Bell state. In contrast, only weak two-qubit correlations are maintained for separable initial states, as entanglement is confined between a single qubit and the field, consistent with monogamy constraints.

The equality given by Eq. (21) is formally analogous to the monogamy saturation observed in the three-qubit W state, implying a vanishing residual tangle and the absence of genuine tripartite entanglement. However, in our system involving an infinite-dimensional bosonic field mode, this relationship does not indicate the absence of genuine tripartite entanglement. The nature of this genuine tripartite correlation is analyzed in detail below.

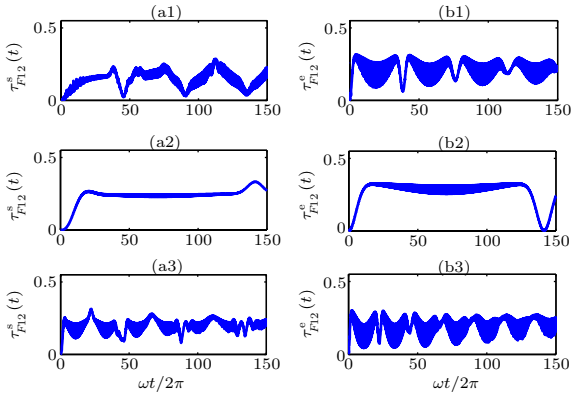


Fig. 4. Time evolution of the I-residual tangle (quantifying genuine tripartite entanglement) for the initial separable (left column) and Bell (right column) states. Panels (a1) and (b1), (a2) and (b2), and (a3) and (b3) correspond to the parameter sets used in Figs. 1–3, respectively.

The I-residual tangle not only characterizes genuine tripartite entanglement but also quantifies the degree of freedom that the system has in satisfying entanglement sharing constraints. This concept, studied in Refs. [42,47], states that entanglement cannot be freely distributed among subsystems in a multipartite system. If $\tau_{ABC}=0$, each bipartite tangle is uniquely determined by the values of all the others; whereas if $\tau_{ABC}>0$, the bipartite tangles have a certain latitude in the values that each can take under entanglement sharing constraints. This reasoning fundamentally relates entanglement sharing to the I-residual tangle. Figure 4 shows the time evolution of tripartite entanglement for two initial states, providing an intuitive manifestation of the freedom in the values of various bipartite tangles under sharing constraints. As shown in Figs. 4(a2) and 4(b2), stable tripartite entanglement is observed in the strong coupling regime at intermediate times, re-

flecting dynamical stability in the latitude of permissible values of bipartite tangles under sharing constraints. $\tau^{e}_{F12}(t)$ vanishes abruptly at $t_1/2$ in Fig. 4(b2), where each bipartite tangle becomes strictly constrained by the values of all the other bipartite tangles. The rapid beat oscillation behavior indicates the continuous redistribution of bipartite tangles required to satisfy entanglement sharing constraints during time evolution.

The strictly positive I-residual tangle confirms the generation of tripartite entanglement in the two-qubit QRM, mediated solely by field-qubit interactions without direct qubit-qubit coupling. Such interactions are pivotal in generating and sustaining different types of entanglement, and circuit QED systems serve as an excellent experimental platform.[20,38,39,48–52] Quantum phase transitions (QPTs) occurring at the critical coupling strength in light-matter systems have been extensively investigated.[21,25,53–56] In particular, there has been growing interest in characterizing these phase transitions from the perspective of entanglement.[57–60] Tripartite entanglement naturally captures richer and more complex quantum information than bipartite entanglement, and thus is expected to possess unique advantages for characterizing QPTs, as singularities in the dynamics serve as unambiguous signatures of the critical point. Consequently, tripartite entanglement can serve as an effective indicator of QPTs in the two-qubit QRM, paving a potential way for further studies.

4. Conclusion

In conclusion, this study presents a comprehensive investigation of entanglement dynamics in the two-qubit QRM. For a system of two identical qubits, we derive analytical expressions for the I-tangles quantifying the bipartite entanglement between the field and the two qubits, as well as between a single qubit-field subsystem and the remaining qubit. These results provide an efficient characterization of entanglement evolution. The nature of the entanglement dynamics depends on the initial state, as the qubit-field interaction either generates entanglement from the separable state or redistributes the preexisting Bell-state entanglement. In the latter case, the initial entanglement exhibits strong robustness against the interaction: the entanglement between the two-qubit subsystem and the field never reaches its theoretical maximum, yet the two-qubit entanglement shows clear periodic revivals. Conversely, generating entanglement between the two qubits starting from the separable state requires both qubit-field coupling strengths to lie within the ultrastrong coupling regime. Crucially, increased coupling strength does not guarantee enhanced entanglement magnitude or stability due to interference among displaced Fock states.

Furthermore, our derivation of the single qubit-field tangle (quantifying a $2\otimes\infty$ subsystem) enables a complete characterization of distinct bipartite entanglement in the two-qubit QRM. These results are crucial for the experimental realization of two-qubit entanglement, quantum logic gates, and the coherent storage and transfer of quantum states in circuit QED and related platforms.

The I-residual tangle quantifies the freedom that different bipartite partitions possess in their pairwise entanglement values under entanglement sharing constraints. The rich dynamical behaviors of the I-residual tangle confirm that qubit-field coupling generates genuine tripartite entanglement. Given the central role of multipartite entanglement in quantum many-body physics, this work paves the way for further exploration of the relationship between genuine tripartite entanglement and quantum phase transitions in the two-qubit QRM. This connection constitutes an important direction for future research.

Acknowledgments

Project supported by the National Natural Science Foundation of China (Grant Nos. 11847111 and 11804246), the Scientific and Technological Innovation Program of Higher Education Institutions in Shanxi, China (Grant Nos. 2019L0822 and 2022L409), and the Natural Science Foundation of Shanxi Province, China (Grant No. 202203021221214).

References

[1] Rabi I I 1936 *Phys. Rev.* **49** 324
[2] Rabi I I 1937 *Phys. Rev.* **51** 652
[3] Scully M O and Zubairy M S 1997 *Quantum Optics* (Cambridge: Cambridge University Press)
[4] Makhlin Y, Scön G and Shnirman A 2001 *Rev. Mod. Phys.* **73** 357
[5] Imamoğlu A, Awschalom D D, Burkard G, DiVincenzo D P, Loss D, Sherwin M and Small A 1999 *Phys. Rev. Lett.* **83** 4204
[6] Jaynes E T and Cummings F W 1963 *Proc. IEEE* **51** 89
[7] Wallraff A, Schuster D I, Blais A, Frunzio L, Huang R S, Majer J, Kumar S, Girvin S M and Schoelkopf R J 2004 *Nature* **431** 162
[8] Chiorescu I, Bertet P, Semba K, Nakamura Y, Harmans C J P M and Mooij J E 2004 *Nature* **431** 159
[9] Bourassa J, Gambetta J M, Abdumalikov A A, Astafiev O, Nakamura Y and Blais A 2009 *Phys. Rev. A* **80** 032109
[10] Forn-Díaz P, Lamata L, Rico E, Kono J and Solano E 2019 *Rev. Mod. Phys.* **91** 025005
[11] Kockum A F, Miranowicz A, De Liberato S, Savasta S and Nori F 2019 *Nat. Rev. Phys.* **1** 19
[12] Qing Y Q, You W L, Lan Y H and Liu M X 2025 *Chin. Phys. Lett.* **42** 020501
[13] Dicke R H 1954 *Phys. Rev.* **93** 99
[14] Leonau A U, San N Q, Ulyanenkov A P, Skoromnik O D and Feranchuk I D 2022 *J. Phys. A: Math. Theor.* **55** 485301
[15] Chen Q H, Wang C, He S, Liu T and Wang K L 2012 *Phys. Rev. A* **86** 023822
[16] Felicetti S, Pedernales J S, Egusquiza I L, Romero G, Lamata L, Braak D and Solano E 2015 *Phys. Rev. A* **92** 033817
[17] Xie Q T, Cui S, Cao J P, Amico L and Fan H 2014 *Phys. Rev. X* **4** 021046
[18] Dong X F, Xie Y F and Chen Q H 2020 *Chin. Phys. B* **29** 020302
[19] Zhu W T, Ren Q B, Duan L W and Chen Q H 2016 *Chin. Phys. Lett.* **33** 050302
[20] Peng J, Zheng J C, Yu J, Tang P H, Barrios G A, Zhong J X, Solano E, Albarrán-Arriagada F and Lamata L 2021 *Phys. Rev. Lett.* **127** 043604

[21] Zhang Y Y, Hu Z X, Fu L, Luo H G, Pu H and Zhang X F 2021 *Phys. Rev. Lett.* **127** 063602
[22] Grimaudo R, Magalhães de Castro A S, Messina A, Solano E and Valenti D 2023 *Phys. Rev. Lett.* **130** 043602
[23] Sun X M, Cong L, Eckle H P, Ying Z J and Luo H G 2020 *Phys. Rev. A* **101** 063832
[24] Yan Z Y, Qu P H, Xu B B, Zhang S H and Ma J Y 2022 *Mod. Phys. Lett. B* **35** 2150213
[25] Grimaudo R, Falci G, Messina A, Paladino E, Sergi A, Solano E and Valenti D 2024 *Phys. Rev. Research* **6** 043298
[26] Albert V V 2012 *Phys. Rev. Lett.* **108** 180401
[27] Giannelli L, Paladino E, Grajcar M, Paraoanu G S and Falci G 2024 *Phys. Rev. Research* **6** 013008
[28] López-Peña R, Cordero S, Nahmad-Achar E and Castaños O 2023 *J. Phys. A: Math. Theor.* **56** 425303
[29] Shi Y Q, Cong L and Eckle H P 2022 *Phys. Rev. A* **105** 062450
[30] Reyes-Bustos C, Braak D and Wakayama M 2021 *J. Phys. A: Math. Theor.* **54** 285202
[31] Li Z M, Ferri D, Tilbrook D and Batchelor M T 2021 *J. Phys. A: Math. Theor.* **54** 405201
[32] Lu X L, Li Z M, Mangazeev V V and Batchelor M T 2021 *Chin. Phys. B* **31** 014210
[33] Nielsen M A and Chuang I L 2010 *Quantum Computation and Quantum Information* (Cambridge: Cambridge University Press)
[34] DiCarlo L, Chow J M, Gambetta J M, Bishop L S, Johnson B R, Schuster D I, Majer J, Blais A, Frunzio L, Girvin S M and Schoelkopf R J 2009 *Nature* **460** 240
[35] Young S M, Jacobson N T and Petta J R 2022 *Phys. Rev. Applied* **18** 064082
[36] He W H, Zhang W H, Yuan X, Shen Y C and Zhang X M 2024 *J. Phys. A: Math. Theor.* **57** 375306
[37] Bhattacharjee A, Jain P, Deshmukh J, Das S, Chand M, Patankar M P and Vijay R 2025 *Sci. Rep.* **15** 4426
[38] Dey A 2025 *Phys. Rev. A* **111** 043705
[39] Huan T T, Zhou R G and Ian H 2020 *Sci. Rep.* **10** 12975
[40] Zhou Y, Xie S Y, Zhu C J and Yang Y P 2022 *Phys. Rev. B* **106** 224404
[41] Wootters W K 1998 *Phys. Rev. Lett.* **80** 2245
[42] Coffman V, Kundu J and Wootters W K 2000 *Phys. Rev. A* **61** 052306
[43] Osborne T J 2005 *Phys. Rev. A* **72** 022309
[44] Mao L J, Huai S N and Zhang Y B 2015 *J. Phys. A: Math. Theor.* **48** 345302
[45] Agarwal S, Hashemi Rafsanjani S M and Eberly J H 2012 *Phys. Rev. A* **85** 043815
[46] Rungta P, Bužek V, Caves C M, Hillery M and Milburn G J 2001 *Phys. Rev. A* **64** 042315
[47] Tessier T E, Deutsch I H, Delgado A and Fuentes-Guridi I 2003 *Phys. Rev. A* **68** 062316
[48] DiCarlo L, Reed M D, Sun L, Johnson B R, Chow J M, Gambetta J M, Frunzio L, Girvin S M, Devoret M H and Schoelkopf R J 2010 *Nature* **467** 574
[49] Devoret M H and Schoelkopf R J 2013 *Science* **339** 1169
[50] Mo X T and Xue Z Y 2019 *Front. Phys.* **14** 31602
[51] Blais A, Grimsmo A L, Girvin S M and Wallraff A 2021 *Rev. Mod. Phys.* **93** 025005
[52] Qi S and Jing J 2023 *Phys. Rev. A* **107** 042412
[53] Baksic A and Ciuti C 2014 *Phys. Rev. Lett.* **112** 173601
[54] Soriente M, Donner T, Chitra R and Zilberberg O 2018 *Phys. Rev. Lett.* **120** 183603
[55] Cai M L, Liu Z D, Zhao W D, Wu Y K, Mei Q X, Jiang Y, He L, Zhang X, Zhou Z C and Duan L M 2021 *Nat. Commun.* **12** 1126
[56] Yang Y T and Luo H G 2024 *Chin. Phys. Lett.* **41** 120501
[57] Xu Y J and Pu H 2019 *Phys. Rev. Lett.* **122** 193201
[58] Gietka K, Chwedeńczuk J, Wasak T and Piazza F 2019 *Phys. Rev. B* **99** 064303
[59] Huang J F and Tian L 2023 *Phys. Rev. A* **107** 063713
[60] Li Y C, Zhou Y H, Zhang Y, Bai Y K and Lin H Q 2024 *New J. Phys.* **26** 023031